UPPSALA
UNIVERSITET

UPTEC F 22003
Examensarbete 30 hp
Jan 2022

# Development of a computational method for determining gamma energy escape from calorimeters at CLAB

Amela Mehic

Civilingenjörsprogrammet i teknisk fysik

UPPSALA UNIVERSITET

Development of a computational method for determining gamma energy escape from calorimeters at CLAB

Amela Mehic

## Abstract

Swedish Nuclear Fuel and Waste Management Company- SKB has conducted measurement campaigns at the Swedish central interim storage facility for spent nuclear fuel- CLAB over the years, extending from year 2003 to 2019 where the gamma energy escape was acquired. At CLAB the spent nuclear fuel assembly is inserted into the calorimeter; device intended to measure temperature increase due to decay heat from the fuel assembly. The calorimetric construction is surrounded by water the medium in which the temperature deviations occur and thus are also measured by the calorimeter. However, there is some leakage of gamma energy from the calorimetric construction and does not contribute to the heating of the water. Therefore, only considering the calorimetric measurements is not enough to estimate the total decay heat in the fuel assembly since these measurements fail to account for the gamma escape.

Measurements of gamma energy escape acquired over the years at CLAB were observed to have some tendencies that where questionable, mainly some stochastic behavior indicating that their uncertainty was profound. In the scope of the thesis a computational method was developed to calculate the gamma energy escape and thus assist in determining which measurements to discard. Combination of two programs were used one being Spent Nuclear fuel- SNF and the second Monte Carlo N particle Simulator- MCNP, to obtain the computational gamma energy escape for different fuel assemblies and cooling times- CTs. It was established that the escape had a range between 1-3,5% and that it had a dependency on CT, fuel assembly type and operational history. Calculated radial exponential decay coefficient for fuel assemblies of the medium; water had also a clear dependency on CT where values of the coefficient increased over CT. Normalized gamma energy distribution over a rotation around the fuel assembly was calculated and it showed that the assembly tended to have the highest radiation coming from its corner rods. The verification of the computational gamma escape results with corresponding measurements yielded that the agreement was quite good for the earlier measurement campaigns. However, deviation became evident after the 2007 campaign where the calculated values were underestimated compared to the measured.

**Teknisk-naturvetenskapliga fakulteten**

**Uppsala universitet, Utgivningsort Uppsala/Visby**

Handledare: Fredrik Johansson, Jesper Kierkegaard Ämnesgranskare: Peter Jansson

Examinator: Tomas Nyberg

# 1 Populärvetenskaplig sammanfattning

Ett hållbart och varaktigt slutförvar av radioaktivt avfall från kärnkraftverk är viktigt för en säker och stabil elproduktion från den svenska kärnkraftsindustrin. Dock står inte kärnindustrin ensam för det radioaktiva avfallet även sjukvård, forskning och annan industri producerar avfall som måste förvaras. I arbetet mot slutförvar hanteras det radioaktiva avfallet från kärnkraftverk i flera steg som liknas vid en kedja. Kedjans startpunkt är då bränslet avlägsnas från självaste reaktorn följt av transport, där destinationen är beroende av avfallets radioaktivitet. För högaktiva avfall är det mellanlagring medan för låg och medelaktiva avfallet slutförvar. Detta projekt avser mellanlagringen av det förbrukade kärnbränslet (CLAB- Centralt mellanlager för använt kärnbränsle). På CLAB utförs mätningar på bränslet i en så kallad kalorimeter; en cylinderliknande konstruktion ämnad att mäta temperaturförändringar orsakade av strålning från bränslet. Under åren har mätkampanjer utförts där gammaenergin utanför kalorimetern uppmätts med gammadetektorer, i syfte att bestämma hur mycket av gammastrålningen som kommer ut från kalorimeterkonstruktionen, nämligen gammaläckaget. Mätningarna som samlats under åren har varierat i storleksordning vilket inte har kunnat förklarats genom fysikaliska skillnader mellan bränsleelementen. Därmed misstänks orsaken ligga i detektorernas funktionalitet och därför är det vikitgt att ha en pålitlig teoretisk modell för att avgöra när detektorerna ger opålitliga resultat.

I det här projektet var syftet att utveckla en beräkningsmetod genom att kombinera två program, nämligen Spent Nuclear fuel-SNF och Monte Carlo N particle Simulator-MCNP. SNF användes för att beräkna andelen gamma av den totala energin hos olika bränsletyper vid olika avklingningstider. Utöver det även extrahera gammaspektrum. Medan programmet MCNP användes för att simulera en modell av bränsle samt kalorimeteruppställning. Genom att definiera källan som antalet gamma fotoner och källans initiala position applicerades Monte Carlo transportkod för att uppskatta fotonernas spridning. På så sätt modellerades ett verklighetstroget scenario och andelen gamma fotoner utanför kalorimetern mot det totala kunde erhållas. Därmed uppskattades hur stor andel av energin som utgjordes av läckaget. Det var inte förrän andelen gammaenergi kombinerades med andelen läckage som det totala gamma-läckaget för bränslet kunde uppskattas.

De beräknade värdena på gammaläckaget var ämnade att bistå i att reda ut vilka av gammaläckagemätningar gjorda på CLAB var mer pålitliga och vilka var mindre. Det som observerades var att senare års mätningar hade större avvikelser från beräkningarna. Medan de tidigare hade en någorlunda bra överenstämmelse.
Projektet resulterade i några viktiga observationer, ett av dem var att totala gammaläckaget hade ett tydligt samband med avklingningstid. Dessutom hade den geometriska konstruktionen av bränslet tillsammans med dess historik en påverkan på storleken av läckaget. Dessa observationer ger en förståelse för vilka parametrar som är viktiga vid uppskattning av gammaläckage från förbrukat kärnbränsle och därmed utgör en grund för vidare analyser.

# Contents

# Nomenclature

### Abbreviations

$BWR$ Boiling Water Reactor

$CLAB$ Swedish central interim storage facility for spent nuclear fuel

$CT$ Cooling Time

$EOL$ End of Life

$GQTH$ Total gamma decay heat

$MCNP$ Monte Carlo N particle Simulator

$NDA$ Non-Destructive assay

$PWR$ Pressurised Water Reactor

$QTH$ Total decay heat

$SNF$ Spent Nuclear fuel

$SKB$ Swedish Nuclear Fuel and Waste Management Company

### Mathematical symbols

A($\varphi$) Radial form function

B(z) Axial form function

D Dose rate

I Intensity

h height

$P_\gamma$ Gamma power escape

r Radial distance

$\rho$ Mass density

$\sigma$ Cross section

V Volume

x Mass thickness

z Cylindrical axis

**Physics Constants**

$\mu$ Attenuation coefficient

$u$ The atomic mass unit

# 2 Introduction

The Swedish model and guidelines for repository of spent nuclear fuel on the basis of international conventions, national law and regulations specifies functions and design considerations in the aim of safety and sustainability. The principle of the final storage arrangement is maintained upon the multi barrier concept, the so called defense-in-depth and the radioactive safeguard principle which is sought to protect from any form of radioactive contamination. Hence avoiding the rise of environmental and health concerns in generation to come. The safety of the storage lay in the use of multi barriers and the bedrock as a geological barrier. The advantage these rock cavities yield in terms of spatial and defence in-depth preservation provide valid contribution to the shielding of the radioactivity. Final faith of all Swedish nuclear fuel is in the attainment of the geological embedment. The repository is substantiated in the resistant canister encapsulation of the spent nuclear fuel, then deposition of the canister at depths of 400-700 m into the crystalline rock cavity at the repository site, surrounded by a protective buffer for prevention of water flow, hence finally back-fill and enclosure of the cavity in the rock[2].

Properties such as the radioactivity of spent nuclear fuel dictates the design, functionality of the repository and is therefore of great importance[2]. The Swedish Nuclear Fuel and Waste Management Company-SKB conduct non-destructive assay (NDA)[1] research and applications at the Central Interim Storage Facility for Spent Nuclear Fuel -CLAB. The analysis is performed through measurements of gamma radiation and decay heat on nuclear fuel assemblies. The primary goals of the measurement are (1)simple and accurate prediction of decay power in the disposal canisters for the spent nuclear fuel by utilizing correlation with gamma measurements, (2)verification of nuclear properties and (3)increase accuracy in determining the total decay power at CLAB[9].

## 2.1 Motivation for the thesis

The long-term goal of safe and secure storage and transport of spent nuclear fuel for the sake of humans, animals and the environment is essential for nuclear industry and its electrical power supply. The significance of radioactive contamination and the devastating affects are not only highly environmental and health concerning, but has the potential in developing into full blown national, in worst case scenario, even international crisis. Therefore the importance of secure, safe and sustainable storage can not be emphasized enough and is always to be pursued.
Proven continuously throughout history that by technical development and safety assessments governing the repository model of spent nuclear fuel, enables successful elimination of risks and achieves the goal. This thesis is intended as a contribution to the technical valuation and achievement of the third stated goal, namely the accurate determination of

[1]Like the name non-destructive states it refers to noninvasive quantitative or qualitative determination of nuclear materials while preserving the integrity of the sample[1].

decay power in fuel assemblies. Also to understand the effect of parameters such as cooling time CT, burnup, spatial distribution and density.

## 2.2 Calorimeter and gamma detectors

A calorimeter submerged in the service pool at CLAB is a device intended to measure[2] the decay heat power in spent PWR and BWR nuclear fuel assemblies.

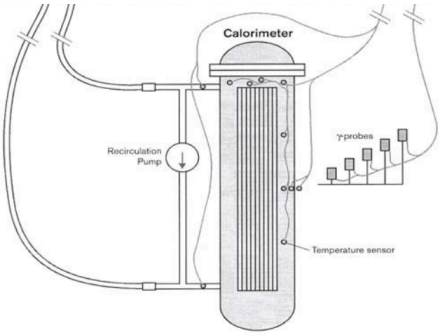


Figure 1: Calorimeter submerged in the service pool at CLAB together with detector prob[9]. Permission to use the figure was granted.

Two parallel cylindrical surfaces confine the calorimeter where the inner referred to as the test chamber has a diameter of 0.33 m and length 4.5 m, see figure 1. The thermal insulator; polyurethane foam fills the space between the test chamber and the outer wall. A fuel assembly is vertically inserted into the calorimeter together with other fuel handling equipment by opening the lid at the top. When closed the lid is an impenetrable barrier between the pool water and the test chamber. Water is circulated by a centrifugal pump in order to preserve the test chambers consistent temperature. However, the calorimetric measurements of decay heat in fuel assemblies are insufficient since there is an escape of gamma energy from the calorimeter construction out into the pool water. This energy escape does not contribute to the temperature rise inside the calorimeter, hence is failed to be detected by calorimetric measurements. In order to increase the accuracy of these calorimetric measurements the gamma energy escape is determined through gamma detection in the water.
Gamma detectors at five different radial positions on a mobile arm construction located outside the calorimeter are intended to measure the gamma energy escape[9].

## 2.3 Gamma spectroscopy measurements of axial profile

In addition to the detector measurements of gamma energy escape, data is also collected from gamma spectroscopy measurements of axial profiles conducted at CLAB. In order to obtain the full axial scan of the fuel assembly; a up and downward motion of the assembly

[2]Calorimetric measurements are defined to be nondestructive measurements of irradiated fuel.

was enabled by using a fuel assembly elevator. The assembly was thus set in motion in front of a high-purity germanium detector positioned initially[3] at a distance of 2.5 m from the center of the assembly. The rotational capability of the elevator equipment allowed for rotations around the assembly axis and thus obtaining scans at different angles, adding the azimuthal dependency on the intensity profile. These gamma-ray intensity profiles for some angles are apprehended in time stamped list mode data [4].

## 2.4 Problem formulation

The performed measurements of gamma dose rate by detectors at CLAB hold a large uncertainty, even stochastic behavior of the detector measurements was seen[6] and does not correctly describe the physical reality. It raises the demand for a computational model which not only yield results that correlate with measurements but also can within some limited uncertainty predict the decay heat of the escape. In the pursuit of determining the decay heat of fuel assemblies, simulation based methods are widely used in obtaining the necessary escape component. However the results from the simulated method need to be verified with appropriate detector measurements.

### 2.4.1 Challenges and difficulties

The challenges that arise are related to the verification stage of the computational method. Due to the already mentioned stochastic behavior and large uncertainty of the measurements acquired over several years. A computational method is used as a reference in order to pinpoint which of the measurement might have some deviations from the computational results due to error or unfamiliar uncertainties. The size of measurement sample also implies statistical limitation in drawing conclusions connected to the sample. It is considered that the measurements that correlate with computations yield not only some indication of which of the measurements might be trustworthy but also that the computational method does in fact have the ability estimate the gamma energy escape. Since having a data set that is not considered reliable imposes difficulties on verifying the correctness of the computational method itself. Also information regarding the existence of fuel assemblies adequate operational history and whether the quality of the measurement is acceptable or not is provided. This information is expected to assist in the explanation of why some measurements might deviate from the computational results.

### 2.4.2 Contribution

The contribution of this thesis is the development of a computational method which is to estimate gamma escape through simulations of the calorimetric set up. A comparison between measurements and computational results is performed. Also the computational

[3]Before the fuel assembly is set in motion by the elevator.

uncertainty at different stages in the estimation is provided as an insight into the accuracy of the method.

# 3 Background and theory of related research

The following section is set out to provide with the physical background and related research needed to comprehend the methods, results and discussions of the thesis. By first defining the attenuation coefficient in section 3.1, which is implemented in the gamma energy escape term of section 3.2. The attenuation phenomena provides some understanding of how the photons are expected to be deflected in the medium. The gamma escape term defines the formula of the experimentally determined gamma escape[4].

## 3.1 Gamma energy attenuation coefficient

Monoenergetic and collimated photon beam with initial intensity $I_0$ irradiates a material with mass thickness[5] $x$ and mass density $\rho$. The exponential attenuation law states that the penetrating photon beam emerges from the material with intensity $I$ and is derived from the following expression,

$$I = I_0 \cdot e^{-(\mu/\rho)x}, \tag{1}$$

where $\mu$ is the attenuation coefficient of the material. Solving equation 1 for the attenuation coefficient

$$\mu = \rho \cdot x^{-1} \cdot ln(I_0/I), \tag{2}$$

where values of intensities $I_0, I$ and thickness $x$ can be measured while material density $\rho$ retrieved from tabulated values[8]. Hence the attenuation coefficient[6] can be derived through equation 2. The attenuation is considered as the fraction of the gamma rays in the collimated beam which do not interact with the material. The probability of interaction which is the cross section is therefore related to the attenuation by

$$\frac{\mu}{\rho} = \frac{\sigma_{tot}}{uA},$$

where $\sigma_{tot}$ is the total cross section for photon interaction, A the relative atomic mass of the target material while $u$ is the atomic mass unit[7]. Total cross section contains all the fundamental photon interactions as the sum

$$\sigma_{tot} = \sigma_{pe} + \sigma_{coh} + \sigma_{incoh} + \sigma_{pair} + \sigma_{trip} + \sigma_{ph.n},$$

where $\sigma_{pe}$ the photo-effect cross section, $\sigma_{coh}$ $\sigma_{incoh}$ the coherent and incoherent cross section respectively, while $\sigma_{pair}$ and $\sigma_{trip}$ the electron-positron production cross section, lastly $\sigma_{ph.n}$ the photonuclear cross section[8].

[4]Meaning the performed gamma detector measurements of the escape at CLAB.

[5]Mass thickness is defined as mass per unit area of the material. It is calculated by traveled distance in material $r$ multiplied by mass density, $x = \rho r$.

[6]There exist numerous tables of attenuation coefficients obtained experimentally, specially in the area of crystallographic.

[7]u=1.660 5402 $\times$ $10^{-24}$g (Cohen and Taylor 1986)

## 3.2 Gamma energy escape term

In the aim of obtaining the total gamma energy radiated in fuel assemblies of spent nuclear fuel at the storage facility CLAB, the escaping decay heat; gamma escape term is derived. It compensates for the insufficiency in the calorimetric measurements of decay heat in the assembly [9]. Hence the escape term is required to be added to the calorimetric determination of decay heat and is calculated as follows

$$P_\gamma = \int_V \rho \cdot D \quad dV, \tag{3}$$

where $P_\gamma$ is gamma escape, $\rho$ the density of the penetrated material, $D$ is the gamma dose rate[8] and $V$ volume[3]. The relative radial distance traveled by the photons in the medium before absorption or attenuation is $(r - r_0)$; from a starting distance of $r_0$ to some arbitrary radial distance $r$. In order to reflect the real geometry of the problem, the integral over the volume elements $dV$ is expressed in cylindrical coordinates. However, the assumption that there is only gamma leakage in the radial directions is made. Hence considering only the radial direction of the gamma distribution, since the dose rate $D$ is approximated as an exponentially depended decay on relative radial distance with attenuation coefficient $\mu$

$$D = D_0 \cdot e^{-\frac{\mu}{\rho} \cdot (r - r_0)}. \tag{4}$$

The initial dose rate $D_0$ in equation 3 is determined by measuring at some distance $r = r_m$ the dose rate $D = D_m$ and then solving the equation above for the initial $D_0$[9][3]. Hence after transforming to cylindrical coordinates and inserting the expression for initial dose rate $D_0$ which includes the measured dose rate $D_m$ at distance $r_m$ equation 3 becomes

$$P_\gamma = \rho \cdot D_m \int_0^h dz \int_0^{2\pi} d\varphi \int_{r_0}^{\infty} e^{\frac{\mu}{\rho} \cdot (r_m - r)} \cdot r \cdot dr. \tag{5}$$

The integrated solution of the equation above yield expression

$$P_\gamma = 2\pi h \rho^2 D_m \cdot (\frac{r_0}{\mu} + \frac{\rho}{\mu^2}) \cdot e^{\frac{\mu}{\rho} \cdot (r_m - r_0)}, \tag{6}$$

which states that the total gamma escape is constant in the finitely large cylinder of height $h$. The source of the gamma energy being the fuel assembly has non homogeneous radiation distribution in both the axial and radial directions respectively. Hence two form functions $A(\varphi)$ and $B(z)$ are considered to compensate for this irregularity [3]. The form functions are weighted quantities that are approximated to be experimentally determined as following,

$$A(\varphi) \approx \frac{1}{n} \sum_{i=i}^{n} \frac{I_{\varphi_i}}{I_{\varphi_{ref}}}, \tag{7}$$

[8]The initial gamma dose rate $D_0$ is defined as the dose rate at the starting distance $r_0$.

[9]The inverse of the dose rate exponential equation is taken to obtain the initial dose rate: $D_0 = D \cdot e^{\frac{\mu}{\rho} \cdot (r - r_0)}$.

$n$ is the number of rotation angles $\varphi$ for which the corresponding gamma intensity $I_\varphi$ is obtained and weighted by the intensity at reference angle $I_{\varphi_{ref}}$[10].

$$B(z) \approx \frac{1}{n} \sum_{i=1}^{n} \frac{I_{z_i}}{I_{z_{ref}}}, \tag{8}$$

The same is said for the axial form function in equation 8 above, where instead of the rotation angle, gamma energy contributions from $n$ axial $z$ components are evaluated and normalized with the reference value. The final expression for calculating the measured gamma escape from a calorimeter at CLAB is therefore

$$P_\gamma = 2\pi h \rho^2 A(\varphi) B(z) D_m \cdot (\frac{r_0}{\mu} + \frac{\rho}{\mu^2})^{\cdot^{\mu(r_m - r_0)}}, \tag{9}$$

with the form functions included[3].

[10]Reference angel is the standard measuring angle used in obtaining the overall gamma heat of the fuel assembly of spent nuclear fuel.

# 4 Methodology for measuring and computing

In the following section the methods used in achieving the results of the thesis are explained; from the measurement acquisition to the computational method. How the computational programs are utilized to derive the significant parameters is presented here, together with the gamma scans which enable experimental determination of the axial and radial form functions.

## 4.1 Dose rate detector measurements

Over the years five different detectors where available during the measurement campaigns at CLAB at which the dose rate was acquired. The calibration and functionality of these detectors varied extensively to the point where in some of the campaigns detectors where dismissed, since they displayed nonphysical behavior yielding negative dose rates or non at all[6]. The gamma dose rate was $D_m$ measured at five radial distances $r_{m1}, r_{m2}, ...r_{m5}$ and through equation 5 yielded a set of independent gamma escape values. However the values where incomplete without the axial and radial form functions in equation 7 and 8 derived by conducting additional measurements. Equation 9 was set to yield the gamma energy escape from the calorimeter, along with some uncertainty being mostly due to the detector uncertainty when measuring the dose rate $D_m$. The value of attenuation coefficient $\mu$ in the equation is independent of the radial range and decay time. Therefore the coefficient was kept constant in equation 9, in the derivation of the gamma escape value at all five detector locations $r_{m1}, r_{m2}, ...r_{m5}$ and different cooling times. Mass density $\rho$ of the pool water is a value considered well known since it is extensively documented and can be found in standard tables of density. In summation; the dose rate was measured at five radial distances from the calorimeter at CLAB and used to derive gamma escape terms through equation 9[9].

## 4.2 Computational Programs

The usage of computational programs in the aim to estimate gamma escape is presented in following section. There are two main computational steps required to achieve the estimation of the escape. The first is the gamma heat ratio; portion of heat generated from gamma radiation and also the energy spectrum, the second; decay heat obtained outside the calorimeter versus the total. In order to fully understand the methodology of these computational programs it is advisable to read through Appendix A and B.

### 4.2.1 Spent Nuclear Fuel Analyses

In order to obtain the total gamma decay heat: GQTH, total decay heat: QTH, photon energy spectrum and nodal burnup distribution of fuel assemblies , STUDSVIK's program for spent nuclear fuel- SNF analyses Version 1.6 was used. For a brief overview and functionality regarding the SNF program see Appendix A.1 for more information. The SNF input is found and explained in Appendix A.2 where decay heat values of fuel assemblies where evaluated

for a set of cooling times and also derived at times of gamma detector measurements. The resulting parameters where extracted from the output file and the ratio GQTH/QTH was calculated as a function of CT. In the case of photon energy spectrum which also varies with decay time and was therefore in the same way retrieved in relation to CT.

### 4.2.2 Monte Carlo N particle Simulator

The gamma energy propagation in the system was simulated by the use of Los Alamos National Laboratory's Monte Carlo N particle transport code Version 5, see Appendix B.1 for more information about the Monte Carlo processes and the estimated error. The photon energy spectrum obtained by SNF was feed into the MCNP input, illustrated in figure 17 of Appendix B.2 where the MCNP cell card commands are outlined. Results of energy deposition over cells that construct the outside geometry of the calorimeter, was extracted from the output file along with the energy sums inside: IN and outside: OUT of the calorimeter. Energy deposition in cells was transformed to yield energy radial distribution by the use of the average cell distance from the center of the calorimeter.The ratio between outside and total energy OUT/TOT[11] was derived and stored for further computations.
Hence key parameters where obtained through SNF and in combination MCNP calculations and are the gamma heat ratio GQTH/QTH in the fuel assembly, energy radial distribution and the outside versus the overall total heat; ratio OUT/TOT of the MCNP model.
Radial exponential decay coefficients where obtained through fitting a first degree polynomial to the energy radial distribution from MCNP inserted into equation 2. The initial deposited energy $E_{r_0}$, considered to be released directly outside the calorimeter wall, along with the deposited energy distributed over radial distance $E_{r_i}$ was computed by MCNP and inserted into equation 2. The leading terms of fitted polynomials yielded values for radial exponential decay coefficients as function of CT with average root mean square error of fit estimated to 0.0053.

A MESH output was enabled by the use of the MESH card, illustrated in MCNP input 16d of Appendix B.2. It superimposes a user defined lattice mesh structure over the constructed MCNP cell geometry and was used in the investigation of fuel assemblies energy deposition distributed over angular and axial space [11].
Angular distributed tally calculations where done for a rotation around the calorimeter where the space was divided into finer cylindrical lattice mesh structures. The energy deposited in each of the mesh cells was calculated by MCNP and the values retrieved from the MESH output. Hence the normalized energy[12] over angle distribution was obtained for certain radial distances from the calorimeter for PWR and BWR fuel assemblies respectively.
Nodal burnup histories of assemblies retrieved from the SNF program where incorporated into the MCNP input where the axial source distribution was no longer uniform as in 16d. Instead the nodal segmentation together with corresponding burnup value where considered

[11] Total energy referred to as the sum of the outside and inside energy of the calorimeter TOT=IN+OUT.
[12] The energy deposited into the mesh cell was normalized with the average energy deposition in all cells.

to approximate the behavior of the axial source. This due to the fact that the axial probability distribution of the particle source was deduced from the burnup values; nodal burnup dividing by total burnup from all nodes. By redefining the particle source and the use of finer mesh lattice cells concentrated axially, the deposited energy distribution was calculated for all four corners of the fuel assembly namely angle 45°, 135°, 225° and 315°. Finally the normalized burnup distribution over axial distance or nodes of the assembly was obtained.

## 4.3 Analysis of gamma-ray axial fuel assembly scans

Gamma spectroscopy measurements of axial profile at angles 45°, 135°, 225° and 315° for multiple fuel assemblies was retrieved from [5], where time stamped list mode data acquisition was performed during measurement campaigns at CLAB. The data files contain a meta-batch divided into list mode event data batches. Characteristics for the event batches is the denoted initial live time followed by the sequence of event channels with corresponding time stamp; real time. The measurements where performed with a certified calibration $^{137}Cs$ source aligned between the detector and the fuel assembly. There where also data sets containing calibration with $^{137}Cs$ and some other background sources acquired after the removal of the nuclear fuel assembly[5].

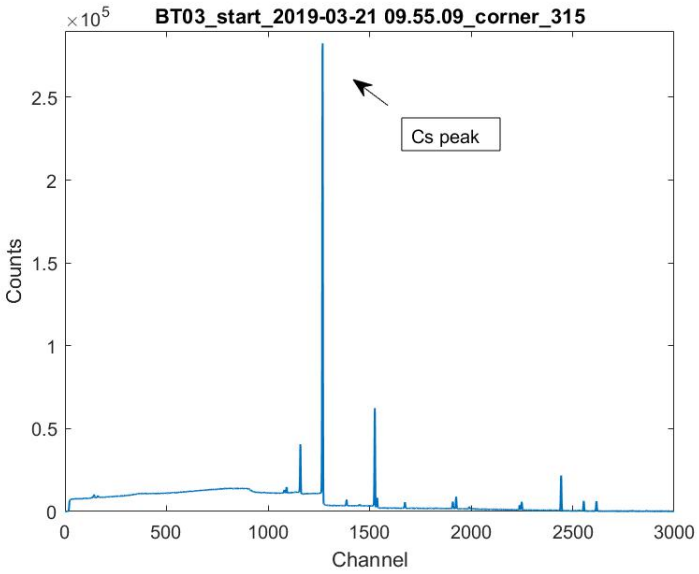


Figure 2: Intensity spectrum of event channels containing the peak of $^{137}Cs$ for fuel assembly BT03 scan at angle 315°.

Event channels which contain the intensity peak of $^{137}Cs$ where retrieved and yielded the total number of counts under the peak[13], see figure 2. The number of occurrences of a specific

[13]The total number of counts or also referred to as gross counts is the integral of the $^{137}Cs$ peak

event channel in the list mode data is directly proportional to the number of counts with energies bounded by the channels energy threshold. The relevant event channels[14] together with the corresponding real times where extracted from the list mode data and the gross counts accumulated into histogram time bins according to their chronological order of detection. The background data set was handled in the same way by accumulating the background counts under the $^{137}Cs$ peak into same number and size of bins; $^{137}Cs$ background count bins. The gross count bins obtained from the fuel assembly data scans were subtracted by the appropriate $^{137}Cs$ background[15] count bins and yielded the net count. The resolution of the final data is connected to the size of the bins where all bins are of the same size. It was observed that a bin size of one second was enough not to lose to much precision and hence destroy the trend of the data. This was seen from plots of count versus time bins where geometrical properties such as the positions of spacer grids in the assembly was inserted. The agreement between the spacer grid positions and the count rate dips was verified and served as assurance that the interpretation of the data was correct, see figure 3.

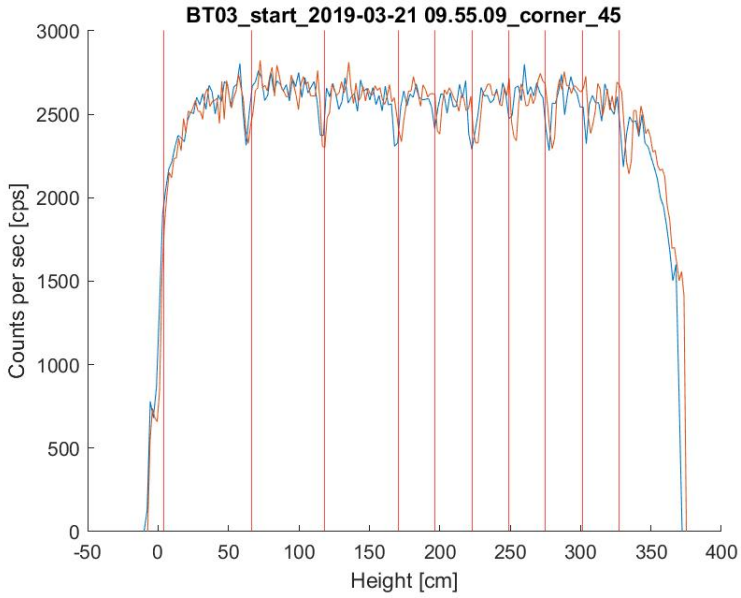


Figure 3: Upward and downward gamma scan of fuel assembly BT03 at angle 45° including an indication of the position of the spacer grids in the assembly.

During the data acquisition the fuel assembly was subjected to a upward motion of about 1.7m/s and thereafter a downward of about 2.1m/s. Hence the fuel assemblies where scanned twice corresponding to the blue and red graph respectively in figure 3. The time axis of the downward scan was scaled to match the time range of the upward scanned time axis. The scaling factor was calculated by dividing the number of time bins for which the net counts

[14]The event channels connected to the $^{137}Cs$ peak are considered to be relevant.

[15]The meaning of appropriate refers to the background measurements acquired closest in time to the fuel assembly scans.

were non zero in the upward scan by the corresponding non zero time bins in the downward scan. Net counts as a function of axial position was obtained by multiplying the upward and the downward scaled time axis with the velocity of the upward motion. Since the scans were acquired in succeeding order on the same time axis the scaled downward scan was therefore shifted and adjusted to overlap the upward scan. The positions of the spacer grids in the fuel assembly are represented by the red vertical lines in figure 3.

### 4.3.1 Form functions

The experimentally determinated axial and radial from function where derived from the list mode data. While the calculated where obtained from the corresponding burnup values with SNF SIMULATE[6]. The axial form function formula was obtained from modifying equation 8 by defining the denominator or the reference intensity as

$$I_{ref,z} = \frac{1}{4} \cdot \sum_{k=1}^{4} \frac{\sum_{i=1}^{n} I_{i,k}}{n},$$

where k(1,2,3,4) = 45°, 135°, 225° and 315° and n the total number of count bins that are non zero or for the calculated the number of data points.

$$B'(z) = \frac{1}{4} \cdot \sum_{k=1}^{4} \frac{2}{n} \cdot \frac{\sum_{i=\frac{n}{4}}^{\frac{3n}{4}} I_{i,k}}{I_{ref,z}}$$

Denotation $B'(z)$ states the reformed axial form function where the numerator is the sum of half the intensity measurements taken around the center of the fuel assembly. The corresponding radial form function derived from modifying equation 7 has the numerator expressed as following

$$I_k = \frac{2}{n} \cdot \sum_{i=\frac{n}{4}}^{\frac{3n}{4}} I_{i,k}.$$

The reference intensity of the modified radial form function defined as the average value of the centered measurements

$$I_{ref,\varphi} = \frac{\sum_{i=\frac{n}{4}}^{\frac{3n}{4}} I_{i,k}}{\frac{n}{2}},$$

finally the radial form function $A'(\varphi)$ is expressed by the following formula

$$A'(\varphi) = \frac{I_k}{I_{ref,\varphi}}.$$

## 4.4 Uncertainty in parameters

Uncertainty in the gamma energy ratio $(\text{OUT/IN+OUT})_{uncer}$ was obtained by the use of equation 10 from Appendix C.1, with the respective uncertainties of the parameters; $\delta OUT$ and $\delta IN$

$$\delta(IN + OUT) = \sqrt{\delta(IN)^2 + \delta(OUT)^2},$$

then equation 11 was applied and the resulting uncertainty obtained:

$$(OUT/IN + OUT)_{uncer} = \sqrt{(\frac{\delta IN}{IN})^2 + (\frac{\delta(IN + OUT)}{IN + OUT})^2} \cdot \frac{OUT}{IN + OUT}.$$

The uncertainty of the radial exponential decay coefficients $\mu_{uncer}$ was calculated by propagating equation 2 through 12 from Appendix section of C.1,

$$\delta(ln(I_0/I)) = \frac{\delta(I_0/I)}{I_0/I}.$$

Since the radial exponential decay coefficients where obtained from the simple linear regression model, the uncertainties where finally yielded from the standard error estimation in equation 13

$$\sigma_\mu = \sqrt{\frac{\sum_{i=1}^{N}(I_0/I - \hat{I_0/I})^2}{N-2}},$$

and thereafter by 14, see Appendix section C.2,

$$\mu_{uncer} = \sqrt{\frac{\sigma_\mu^2}{\mu}_{uncer} \sum_{i=1}^{N} x_i^2 - N \cdot \bar{x}^2}.$$

Lastly the normalized energy over angle uncertainty $(\text{E/E}_{avg})_{uncer}$ was calculated by extracting the uncertainty of deposited energy in cell $\delta E_i$ from MCNP outputs. Thereafter the normalization factor was calculated through estimating the uncertainty of the mean value

$$\delta E_{avg} = \sum_{i=1}^{N} \frac{\delta E_i}{N},$$

and hence propagating through the ratio

$$(E/E_{avg})_{uncer} = \sqrt{\delta E_i^2 + \delta E_{avg}^2},$$

resulting in the final uncertainty of normalization.

# 5 Results

The spent fuel assemblies investigated through the use of their operational histories[16] are from Ringhals reactors BWR: R1, PWR: R2, R3, R4 and Forsmark BWR: F1, F2 and F3. The aim was not only to conduct computations estimating the gamma leakage[17] in these assemblies but also to understand the dependencies on parameter such as CT, burnup, spatial distribution and density. Also through the computational method calculate the usually experimentally determined axial and radial form functions. The following section presents the results obtained in the scope of the thesis.

## 5.1 Computational results

In the section below results obtained from the computational method developed throughout the course of the thesis are presented. Distinction between the fuel types BWR and PWR and also their corresponding assembly models are made for the purpose of better understanding, observing trends and dependencies governed by the geometrical construction of the fuel.

### 5.1.1 Gamma ratio and total escape dependence on CT

Figure 4 is composed of two parametric quantities and their dependence on CT respectively. The ratio OUT/IN+OUT meaning the proportion gamma energy outside the calorimeter and the total gamma escape (OUT/IN+OUT)×QG/QGTH. Two important distinctions are made; the solid line representing the expected behavior of the parameters over a range of CT and the dots, which are computational values of the measurements at CLAB. Each solid curve represents a fuel assembly denoted with the assemblies reactor; R1, R2, R3, R4, F1, F2, or F3 and assembly ID while the dots representing measured fuel assemblies denoted with assemblies reactor and model, see section B.3. The uncertainty propagation of total gamma escape from different BWR and PWR fuel assembly models is presented in figure 5 as a function of CT.

[16] Information regarding the operation of the fuel during its lifetime; irradiation, number of fuel cycles, moderator properties etc.

[17] Gamma energy escape outside the calorimeter.

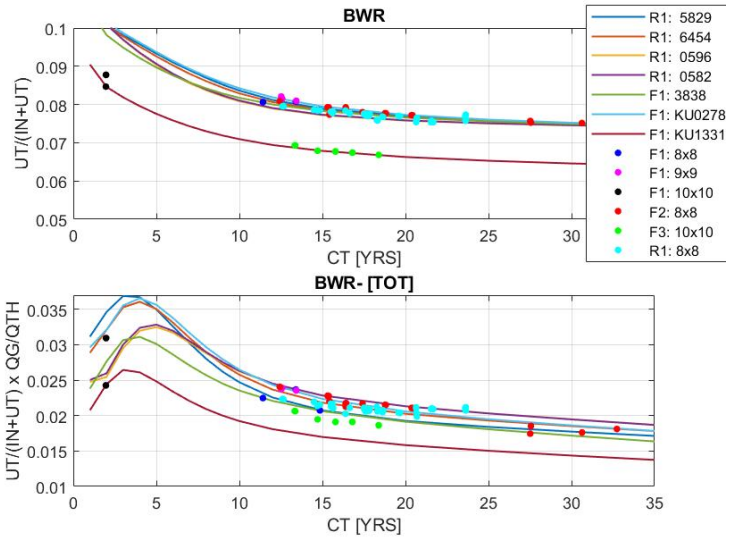


(a) BWR fuel assemblies

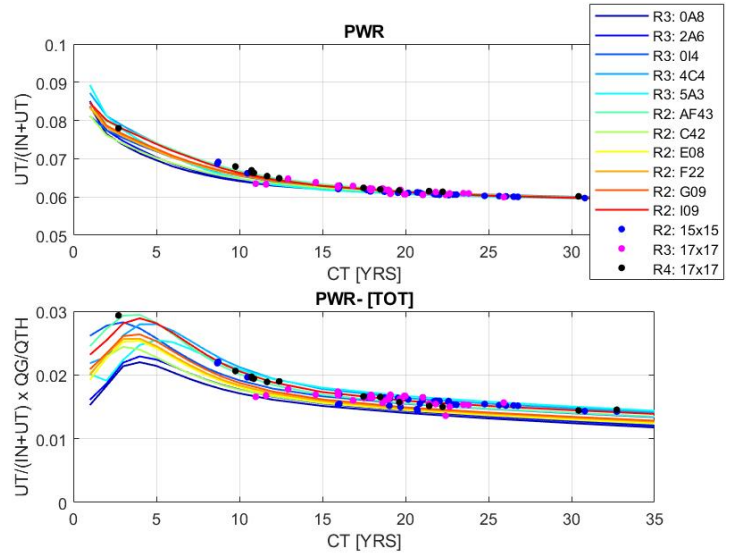


(b) PWR fuel assemblies

Figure 4: a) Value of the ratio gamma outside calorimeter over CT b) The total gamma escape over CT.

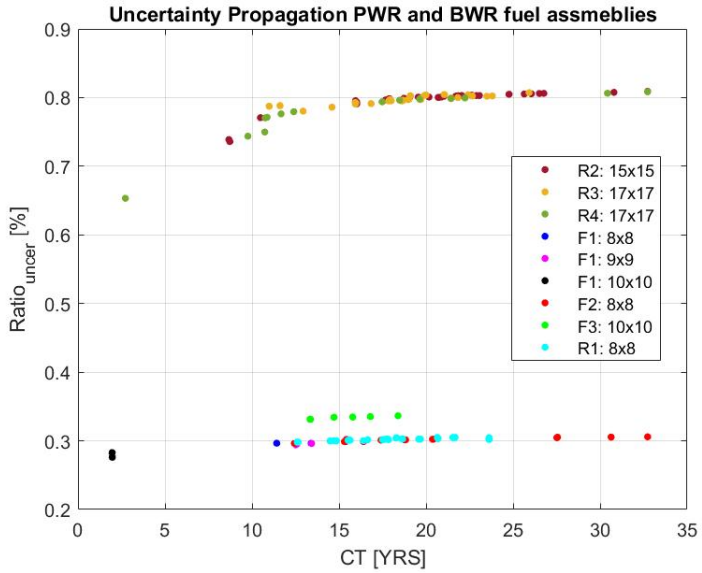


Figure 5: Uncertainty of the computationally determined gamma ratio: OUT/IN+OUT.

### 5.1.2 Gamma ratio, total escape and radial exponential decay coefficients dependence on density

Figure 6 depicts the PWR fuel assembly from Ringhals reactor 2: R2 and how its gamma ratio, total escape values and decay coefficients depend on density of polyurethane insulator foam.

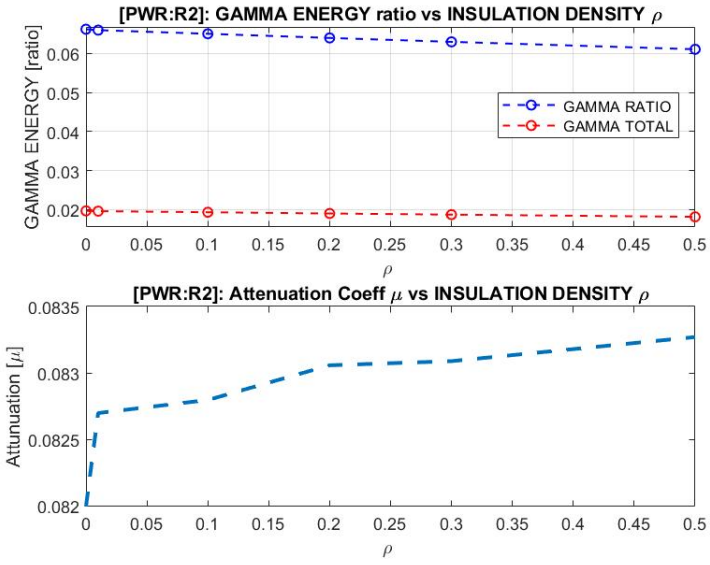


Figure 6: [Above] Gamma ratio and total gamma escape, [Below] decay coefficients dependence on insulator density of polyurethane foam in the calorimeter wall.

### 5.1.3 Radial exponential decay coefficients dependence on CT

Computationally determined radial exponential decay coefficients and their dependency on CT for different BWR and PWR fuel assembly models is seen in figure 7. Their uncertainties are presented in figure 8.

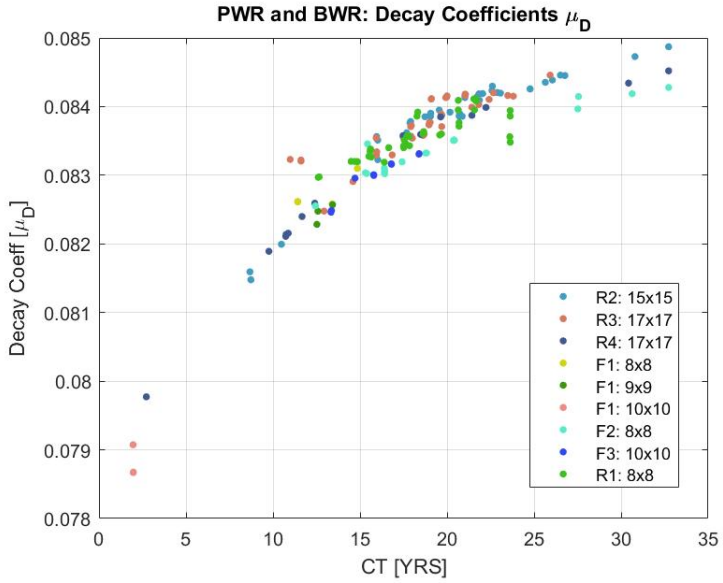


Figure 7: Radial exponential decay coefficients of PWR and BWR fuel assembly models as a function of CT.

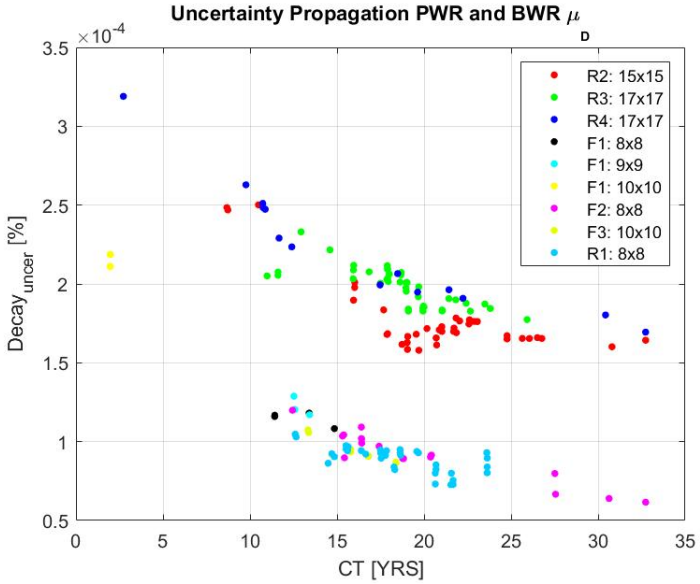


Figure 8: Uncertainties of fuel assemblies radial exponential decay coefficients in figure 7.

### 5.1.4 Normalized gamma energy distribution over angle

The MCNP MESH results yield gamma energy ratio or normalized gamma energy dependency on angle, illustrated in figure 9 for some radial distances from the calorimeters outer wall. The uncertainty propagation for the BWR and PWR fuel assembly distributed over a rotation around the assembly is seen in figure 10.

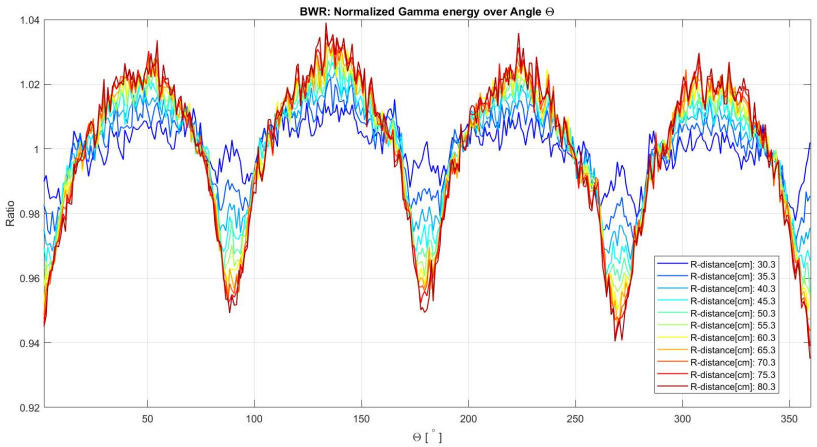


(a) BWR fuel assemblies gamma energy ratio for some radial distances over one rotation.

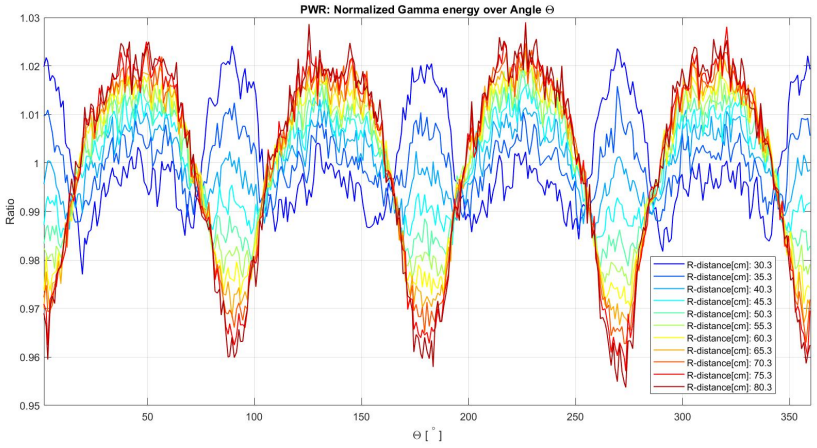


(b) PWR fuel assemblies gamma energy ratio for some radial distances over one rotation.

Figure 9: The ratio of gamma energy distributed over a rotation about the fuel assembly for some radial distances from the calorimeter.

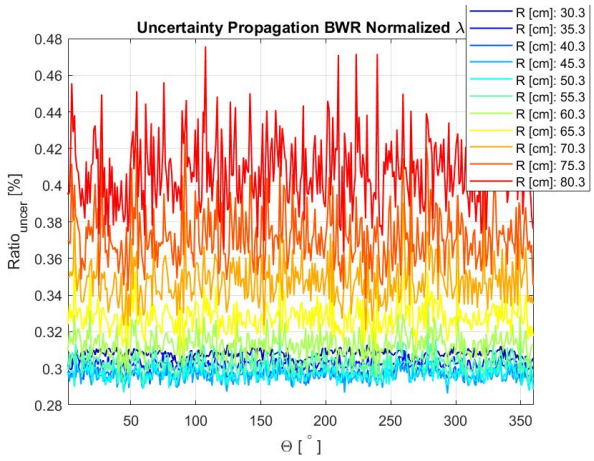


(a) Uncertainty of gamma energy ratio for BWR fuel assemblies.

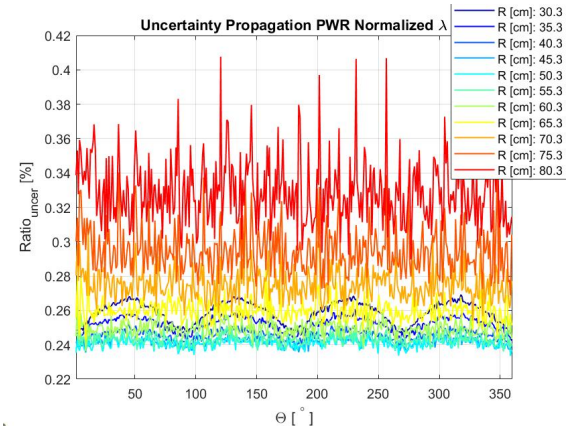


(b) Uncertainty of gamma energy ratio for PWR fuel assemblies.

Figure 10: Uncertainty of the gamma energy ratio in figure 9 for BWR and PWR fuel assemblies respectively.

## 5.2 Measurements of total gamma energy escape

In the following section, measurements of total gamma energy escape conducted at CLAB are presented in two different ways. The reason for the excessive representation is to illustrate the different aspects of the data. In figure 11a the spread in data over the years in which the measurements where conducted is emphasized while for 11b the trend related to the different fuel assemblies. The years in which the measurement campaigns in figure 11b where conducted are found in table 1.

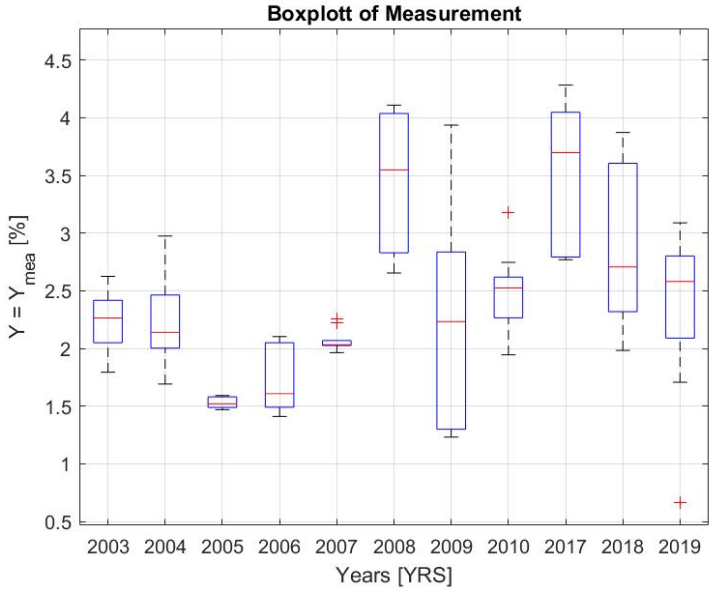


(a) Box plot of gamma escape measurements conducted over the years at CLAB.

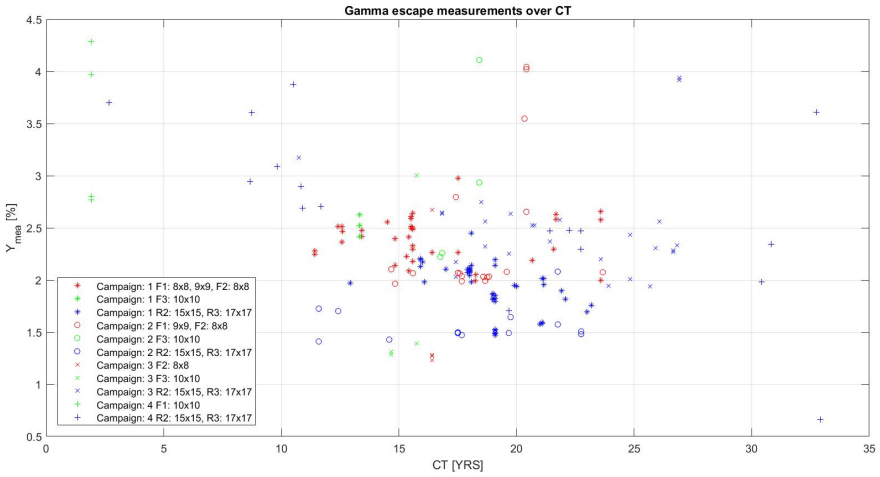


(b) Gamma escape measurements divided into different campaigns and fuel assembly models.

Figure 11: Detector measurements of gamma energy escape from calorimeter at CLAB.

Table 1: Measurement campaigns from figure 11b together with the years in which they where performed.

| Campaign | Year |
|---|---|
| 1 | 2003, 2004, 2005 |
| 2 | 2006, 2007, 2008 |
| 3 | 2009, 2010 |
| 4 | 2017, 2018, 2019 |

## 5.3 Computational versus measured total gamma escape

The ratio of computed total gamma escape of figure 4 through measurements, distributed over CT and years respectively, is seen in figure 12a. Their relative error is presented in figure 12b. Distinctions are made based on some background information regarding the measured assemblies operational histories, measured qualities or both.

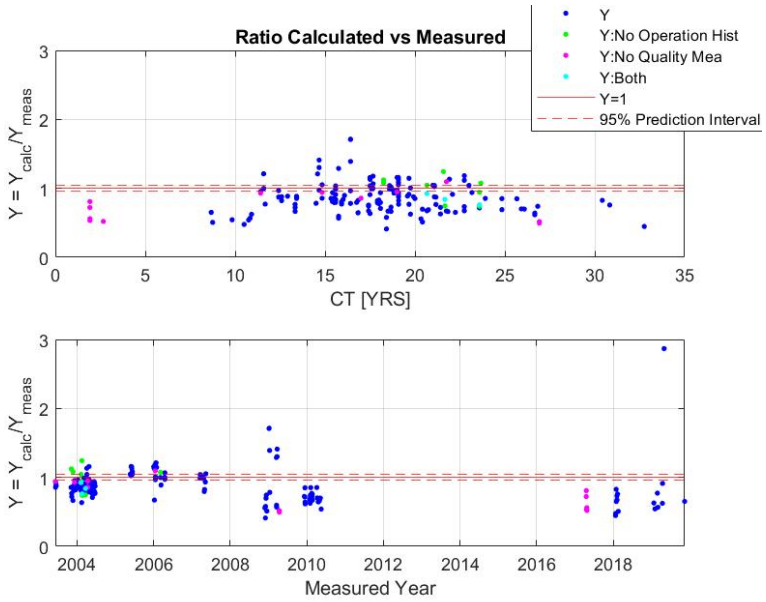


(a) Ratio between calculated and measured total gamma energy.

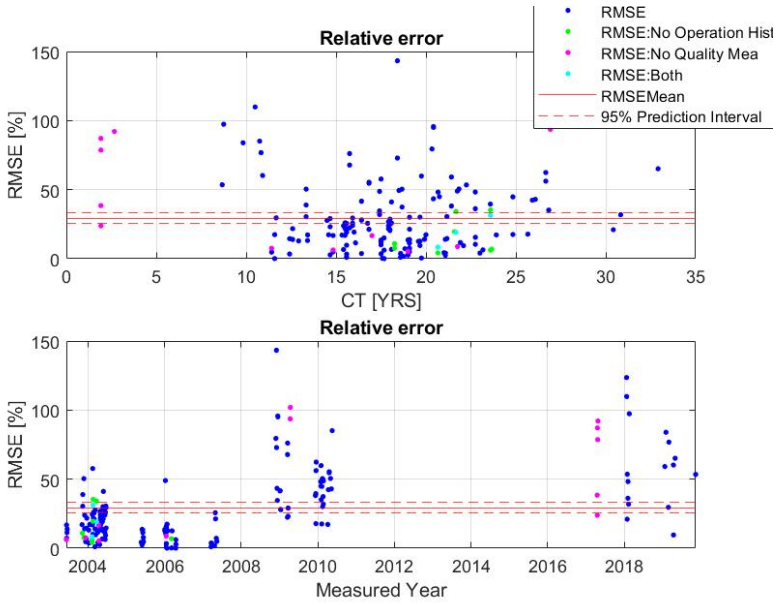


(b) Relative error between computational and measured values.

Figure 12: Relation between computationally determined total gamma energy and measured together with the relative error.

## 5.4 Computational versus measured form factors

The averaged experimentally determined axial form factors and the corresponding calculated from factors are presented in the first part of figure 13 for two PWR and three BWR fuel assemblies. Averaged experimentally determined along with calculated radial form factors for PWR and BWR fuel assemblies distributed over the corner of the assembly are seen in the second part of figure 13. The first pair of bars from the left side of the figure are the experimentally determined and calculated form factors of the first PWR assembly seen on the horizontal axis of the figures first part. The second pair represents the experimental and calculated radial from factor of the second PWR assembly and the third pair of bars yields the form factors of the first BWR assembly and so on.

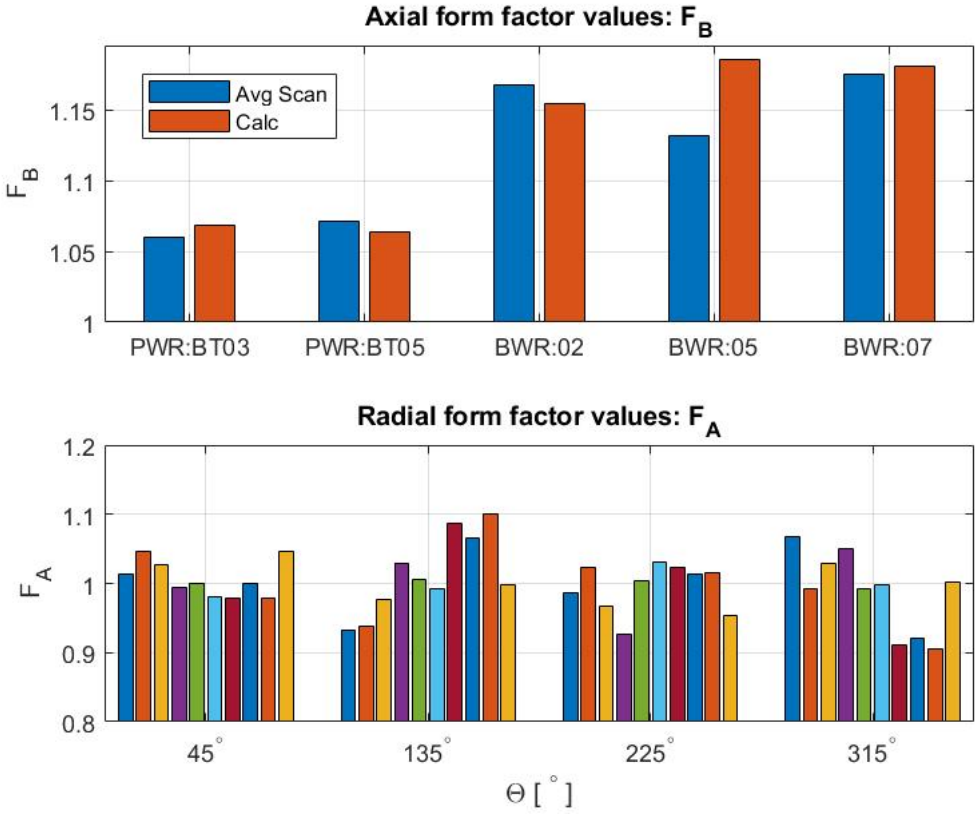


Figure 13: [Above] Average and calculated axial form factor. [Below] Average and calculated radial form factor distributed over angles around the BWR and PWR fuel assemblies.

# 6 Discussion

In the ensuing section the results presented in section 5 are discussed along with their associated uncertainties. The purpose of these discussions is to understand the nature behind the trend of the resulting data. If any difference exists between BWR and PWR fuel assemblies explain its origin by the difference in the geometrical construction. The verification of the computations with measurements and vice versa are also discussed.

## 6.1 Gamma ratio and total escape dependence on CT

The computationally determined ratio of gamma energy outside the calorimeter follow the trend of the expected ratio derived for a set of CTs in the interval of 1-35 years. This is seen in figure 4 where the computed ratio of different BWR and PWR fuel assembly models agree well with the expected ratio; solid curve.
In the second part of figure 4a and 4b the total gamma energy escape of the expected and computed have overall good agreement. However it is somewhat worsened in comparison to the gamma energy ratio. This is mostly true for the BWR fuel assembly models where the scattering of the curves is greater than for PWR. It is also noted how the computed F3: 10x10 values do not align with its corresponding expected curve.
The worsened agreement of total gamma energy escape between the computed and computationally expected values is explained by the unknown uncertainty in the total gamma decay heat QG/QTH derived by SNF. This factor contributes to the increase in uncertainty of the parameter and therefore worsening the agreement. The total gamma energy decay heat does not exist in the gamma energy ratio hence not causing this problem. It would be of great interest to investigate the uncertainty from SNF output to see if this really is the case. However at the moment there is no straightforward way of obtaining the information required to derive the uncertainty from SNF.
The scattering of expected total gamma escape, especially between fuel assemblies of the same model such as R1: 8x8 in figure 4a, is due to the fact that their operational histories are different. Even if there is a similarity in geometrical construction of the fuel, the difference in operational and irradiation history is manifested in the decay heat factor QG/QTH causing the deviation to be inevitable.

The gamma energy escape ratio is overall greater for the BWR fuel assemblies except for the 10x10 model which has a level similar to the PWR. This is explained by the number of uranium rods constituting the assembly. Although radiating gamma energy they also act as a shield due to their high densities. The escaping gamma rays are therefor considered to originate from the outermost rods since the more centered are likely shielded off. The BWR fuel assemblies seen in figure 18 of Appendix B.3 have fewer fuel rods located in the middle of the assembly. Hence less rods are subjected to the screening affect from the rods at the boundary. The PWR fuel assemblies have more fuel rods and naturally more of them are centered thus a greater portion is subjected to the screening. It is therefore considered

that the ratio of shielded fuel rods increases with the total amount of fuel rods or size of the assembly which result in a lower level of gamma energy escape.

## 6.2 Gamma ratio, total escape and radial exponential decay coefficients dependence on density

The density of polyurethane insulator foam in the calormeter wall at CLAB is somewhere between 0.01 - 0.1 g/cm$^3$. In figure 6 the ratio gamma energy and total escape is seen to have a slightly increasing slope. The derivative of this function is considered to be close to zero over the corresponding density range of the real life scenario. For the ratio this deviation is 0.094% and it is even less for the total escape 0.028%. Therefore the dependency on the density of the insulator is negligible and hence does not affect the parameters in any significant way. The same is said for the radial exponential decay coefficients in the second part of the figure where the deviation over the range is 0.0097% concluding that any impact imposed from the change in density is discarded. The investigation was done for a PWR: R2 15x15 fuel assembly. However, one can argue that similar results would be obtained from BWR fuel assemblies. Partly due to the parametric values having the same shape over CT regardless of operational history, fuel type and model seen in figure 4.

## 6.3 Radial exponential decay coefficients dependence on CT

Radial exponential decay coefficients of different fuel assemblies are observed to clearly have dependency on CT, figure 7. Supposedly due to the gamma energy spectrum dependency on CT. Since the energies are expected to vary over time due to the numerous decay chains of different isotopes in the spent nuclear fuel. The shape of the alignment reminds somewhat of the logarithmic function. Indicating that the constant value used for the attenuation coefficient in deriving the measured gamma escape through equation 9, might no longer be considered an adequate approach. Instead it is believed to contribute in the systematic error of the measured total gamma energy escape. In order to avoid this the CT dependency needs to be take into consideration which primarily means using different radial exponential decay coefficients for different CTs. One fails to find any deviation patterns between the coefficients of BWR and PWR assemblies and hence it is believed that it does not exist. Alternatively that a more extensive investigation with a larger data set of assemblies is required.

## 6.4 Normalized gamma energy distribution over angle

An oscillating behavior is seen in figure 9 where the energy ratio or normalized energy is projected over a rotation around the fuel. Due to the symmetry of the fuel assembly the oscillation is expected. At angles facing the corners of the fuel; fuel rods on each side of the assembly are equally in the field of view. The accumulated radiation from both sides causes the increase in gamma energy. This becomes evident since in most cases the corners are seen to release relatively more energy. The field of view increases with distance from the corner,

hence more fuel rods become visible while the relative distance between the rods becomes more insignificant. This causes a greater release of energy further away from the calorimeter in the direction of the corners. Also observed as increase in amplitude of the oscillation with radial distance.
An additional 45° rotation from the corners and the reverse becomes apparent; more of the energy is released closer to the calorimeter, since the field of view is changed to face the flat side of the assembly. Unlike before the increase of the field does not imply that more fuel rods are visible. Hence there is no such accumulation of radiation over distance instead there is a decrease over distance. However, the PWR fuel assembly in 9b has greater energy releases at angles directly parallel to this side than the BWR in 9a. Due to the PWR fuel assemblies greater size it contains more fuel rods in its boundary than BWR. Therefore with more fuel rods radiating gamma energy in these directions, more energy is seen.

## 6.5 Measurements of total gamma escape

Figure 11a illustrates the dispersion of measurements for each year based on minimum, first quartile, median, third quartile and maximum values. The red pluses seen above or below a boxplot are outliers which represent some small portion of remaining data failed to be captured by the box. It is observed that later measurements seem to have an overall greater spread in data. Initially dispersion does not indicate unreliable measurements since they represent different fuel assembly models with different operational histories, hence are expected to have distinctions in total gamma energy escape. However the questions is how large of a dispersion is acceptable due to geometrical and operational differences of the fuel. The corresponding computational results of figure 4 confirms the existence of this dispersion. However, it suggests that the spread is to big in some of the later conducted measurements.

Measurements are projected over CT in order to see if the trend of figure 4 is observed. The median of the measurements in figure 11b is expected to follow the trend of figure 4 quite well. It seems that measurements of shorter CTs have overall higher values and somewhat exponentially decline towards the center. The measurements in 11b confirm the behavior of the corresponding computational results. However, the dispersion between individual measurements is considered to great to confirm this with high certainty. Also the amount of data is insufficient especially for lower and greater CTs in order for these claims to be anything other than speculations. Therefore the conclusion is the following; although the possibility does exist that some of the measurements follow the same trend as the computed gamma escape, they are superimposed by the ones that do not. Since the data sample is scarce it becomes difficult to pinpoint with higher accuracy which ones do.
The median of the measurements in figure 11b is expected to follow the trend of figure 4 quite well. The measurements confirm the behavior of the corresponding computational results. However the dispersion between individual measurements is considered to great to confirm this for certain.

## 6.6 Computational versus measured total gamma escape

The verification of the calculated gamma escape against the measured is presented in figure 12a in the form of the ratio between these two results. The ratio serves as an indication of how well the measured agree with the calculated by how close to value 1; observed as the red horizontal line in the figure, these ratio values align. The deviation from this line is hence considered to indicate the opposite mainly that the agreement is off by the factor of the ratio. Relating the calculated and measured gamma energy escape in this way yields a measure of the agreement. It is observed from the first part of the figure that most of the data has CTs in between 10-25 years, as a consequence of this the overall agreement is higher there. Since there is more data within this CT range the probability of obtaining ratio values closer to 1 is higher than for the lower or greater CTs where the data is scarce. In the second part of the figure the same ratio values are presented however they are distributed over the time of the measurement acquisition. It is clearly seen that the deviation from the horizontal line is greater for the later measurements, after the measurement campaign of year 2007. The previous campaign values are aligned quite well in relation to the later. Since the calculated gamma escape results are expected to have somewhat constant uncertainty, indicating that it had to be the measurements that where subjected to an increase in uncertainty in the later measuring campaigns. This is also seen by the relative error illustrated in figure 12b where the later measurement campaigns have higher error than the earlier.

## 6.7 Computational versus measured form factors

Experimentally determined averaged and calculated axial and radial form factors are seen in figure 13. The averaged axial and radial form factors are derived by using the gamma spectroscopy measurements of axial profile in section 4.3. Form factors are obtained through the formulas outlined in section 4.3.1. An experimentally determined form factor is calculated for each scan; upward and downward of the fuel assembly profile and then averaged over these two scans. Nodal burnup distribution for each corner of the assembly is used in the definition of form functions in section 4.3.1 in order to obtain the calculated form factors.
In the first part of figure 13 the axial form factors are presented and experimentally determined and calculated are compared. It is seen that all form factors are greater than value one which indicates that radiation from fuel assemblies are non homogeneous in axial directions. The PWR axial form factors are also seen to be significantly lower than the BWR which is expected due to PWRs lower nodal burnup. The computations and the experimental form factors are seen to agree somewhat however for assembly BWR:05 the deviation is greater. This is considered to be explained by an insufficiency in the calculation, since it is the calculated form factor value that differs from the other two BWR assemblies and not so much the experimental.

The second part of figure 13 the experimentally determined and calculated radial from factors are presented over the corners of the assembly. It is noted that there is a overall good agreement between experimental and calculated radial form factors mostly at angle 45°.

However there is also deviations which there is no obvious cause for; due to the intensity profile measurements used in deriving the experimental form factor or some insufficiency in the calculations with nodal brunup. The deviations seen are considered not to be extreme since the maximal deviation between an experimental and calculated result is 0.1 and the minimal 0.005. Even do using the calculations to estimate experimentally determined radial from factors is considered to be insufficient since there is no way to determine the accuracy of the estimation if the two are not compared.

## 6.8 Uncertainty of calculated and measured results

The uncertainty of the computed gamma energy ratio is presented in figure 5, where BWR have considerably lower uncertainties than PWR assemblies. The explanation lays in the run time of the MCNP program for which the accuracy increases with time. Hence the lower uncertainty values of BWR are the results of the longer run time of the MCNP inputs. Still the uncertainties for both of the fuel assembly types; BWR in the range of 0.27-0.31% and PWR 0.65-0.81% are considered relatively low and therefore longer run times are not needed. Additional approximations done during the calculations along with the unknown uncertainty from the SNF calculations of the gamma decay heat are also considered to have contributed to the uncertainty of the computed total gamma energy escape.
The uncertainty propagation of results in figure 7 derived by following the calculations in section 4.4, is seen to have an exponential decline over CT; figure 8. The reason for this is probably due to the uncertainty propagation inside the logarithmic definition of attenuation coefficient; equation 2. The coefficients are calculated from fitting a fist degree polynomials to values of gamma energy ratio obtained from MCNP outputs. The uncertainties are therefore calculated by the standard error estimation in section 4.4.
Figure 10 comprised of the systematic and the profound random error of the normalized gamma energy projected over a rotation around the fuel. The drastic alterations are believed to be white noise while the amplitude of the uncertainty, seems to increase somewhat with radial distance. These random and unpredictable fluctuations when trying to determine the uncertainty, are believed to originating from the propagation of noise inside the normalized energy of figure 9. There is a trade off between apprehending good statistical representation of the energy at greater distances and run time of inputs. Since attenuation becomes more likely and hence less of the initial gamma energy reaches these distances. The price of not having enough data to describe the system is the cost in accuracy.

The uncertainty in the measurements of gamma energy escape lays primarily in the calibration of the detectors and and also their efficiencies. Since there is a discrepancy in the calibration of individual detectors at CLAB and deterioration due to the irradiation in the pool water, it was through the gamma escape measurements detector deficiency was noticeable. Therefore these detector uncertainties are hard to quantify since their origin can only be speculated and hence even less so quantified. The fail to consider the radial exponential decay coefficients dependency on CT in obtaining the escape through equation 9 is consider

to additionally contribute to the uncertainty in the measurements, along with the detectors. In further investigations; the error caused by not accounting for the variations of radial exponential decay coefficients due to CT can be derived in order to apprehend some understating of its magnitude.

# 7 Conclusion

The total gamma escapes dependency on CT, operational history and geometrical construction of the fuel assembly is evident. The ratio of shielded fuel rods increases with assembly size resulting in a gamma escape decrease. Gamma energy ratio, total escape and radial exponential decay coefficients are not dependent on density of the polyurethane insulation foam. However, the computed radial exponential decay coefficients are dependent on CT. This needs to be accounted for when obtaining the gamma energy escape measurements from equation 9. The corners of the fuel assembly tend to radiate the greater portion of the gamma energy. At the earlier measurement campaigns, before year 2008 the acquired measurements had overall better agreement with the computed gamma energy escape than the later ones. However more measurements with lower and greater CT are required in order to have a better representation of the data sample.

# 8 Future work

In further development of the thesis it is advisable to obtain a larger data sample. Meaning the gamma energy escape is to be calculated using the obtained computational method derived throughout the scope of the thesis, along with measurements done by gamma detectors at CLAB, for a greater number of fuel assemblies with different ranges of CTs. This in order to obtain higher statistical accuracy and hence increase reliability. It would be of great interest to further investigate the uncertainty of the measurements done at CLAB. To try and find the reason behind the stochastic behavior and also why the later measurement campaigns, have poorer agreement with the computational results of the gamma escape. Try and pinpoint the detectors contribution to the measured uncertainty. Also determine the uncertainty from SNF results since it is expected to increase the overall uncertainty of the computational results.

# 9 Acknowledgments

With this thesis I complete my Engineering in Applied Physics degree at Uppsala University. The project was done in collaboration with the Swedish Nuclear Fuel and Waste Management Company- SKB. Thereby, I would like to express my gratefulness to have been given the opportunity of being a part of their work.

It is with great gratitude that I thank my supervisors Fredrik Johansson and Jesper Kierkegaard at SKB for their time, guidance and constant support. Whom also provided me with knowledge and tools that enabled the results of this thesis. It has been a pleasure to work with you.

To my subject reader Peter Jansson for not only correcting this report but also for his advise and helpfulness throughout the project. I am grateful towards your commitment and constructive feedback.

Finally to my family and friends, I appreciate everything you have done for me and your support throughout the good and the bad.

# References


[1] Los Alamos National Laboratory A. GAVRON. "NONDESTRUCTIVE ASSAY TECHNIQUES APPLIED TO NUCLEAR MATERIALS". In: *The International Nuclear Information System* (July 2001), pp. 1–7. URL: https://inis.iaea.org/collection/NCLCollectionStore/_Public/33/007/33007959.pdf.

[2] Svensk Kärnbränslehantering AB. "Design and production of the KBS-3 repository Technical Report TR-10-12". In: (Dec. 2010), pp. 1–56. URL: http://www.skb.com/publication/2167363/TR-10-12.pdf.

[3] Martin Bengtsson and Peter Jansson. "KBP6003 - Methodology for Assessment of Calorimetric Measurement with the Temperature Rising Method". In: 1 (2020), pp. 1–5. ISSN: 0092-640X. DOI: 10.1016/j.adt.2011.12.006.

[4] Peter Jansson. "Axial and Azimuthal Gamma Scanning of Nuclear Fuel – Implications for Spent Fuel Characterization". In: *Journal of Nuclear Materials Management* 45.1 (2016), pp. 34–47. ISSN: 0893-6188. URL: https://resources.inmm.org/system/files/jnmm/vol_45/V-45_1.pdf.

[5] Peter Jansson et al. "Time stamped list mode data from gamma-ray spectroscopic measurements on 47 nuclear fuel assemblies performed at Clab, Sweden, September 2016 through March 2019". In: 31.10 (Aug. 2020), pp. 1–9. ISSN: 106039. URL: https://doi.org/10.1016/j.dib.2020.106039.

[6] Svensk Kärnbränslehantering-SKB. Presentation of collected measurements over the years at CLAB. Aug. 2021.

[7] Tom O'Haver. "Error Propagation in Arithmetic Calculations". In: *Department of Chemistry and Biochemistry* (2020), pp. 1–1. URL: https://terpconnect.umd.edu/~toh/models/ErrorPropagation.pdf.

[8] National Institute Standards and Technology. *X-Ray Mass Attenuation Coefficients*. URL: https://physics.nist.gov/PhysRefData/XrayMassCoef/chap2.html.

[9] Fredrik Sturek and Lennart Agrenius. "Clab– Measurements of decay heat in spent nuclear fuel assemblies". In: 1 (2021), pp. 5–16. ISSN: 1402-3091. URL: https://www.skb.se/publikation/1472024/R-05-62.pdf.

[10] X-5 Monte Carlo Team. "MCNP — A General Monte Carlo N-Particle Transport Code, Version 5 Volume I: Overview and Theory". In: 1.5 (2003), pp. 1–416. URL: https://mcnp.lanl.gov/pdf_files/la-ur-03-1987.pdf.

[11] X-5 Monte Carlo Team. "MCNP — A General Monte Carlo N-Particle Transport Code, Version 5 Volume II: User's Guide". In: 1.5 (2003), pp. 1–508.

[12] Sheldon M. Jeter Georgia Institute of Technology. “APPLICATIONS OF ERROR PROPAGATION ANALYSIS TO THE UNCERTAINTIES OF REGRESSION MODELS IN EXPERIMENTAL THERMAL AND FLUIDS ENGINEERING”. In: *American Society for Engineering Education* (2002), pp. 1–18. URL: https://terpconnect.umd.edu/~toh/models/ErrorPropagation.pdf.

[13] Harvard University. “A Summary of Error Propagation”. In: (2007), pp. 1–5. URL: http://ipl.physics.harvard.edu/wp-uploads/2013/03/PS3_Error_Propagation_sp13.pdf.

[14] Studsvik Scandpower USA. “SNF User’s Manual”. In: 1.11 (2020), pp. 1–148.

# Appendix

# A STUDSVIK's System for Spent Nuclear Fuel Analyses Version 1.6

## A.1 Overview

Spent Nuclear Fuel- SNF Analyses computer system derives isotopic concentrations, radiation source terms, total and gamma decay heat, photon spectra, total activity of fuel assemblies or individual fuel rods at the time of discharge or after some given cooling time-CT. The nodal segmentation of the fuel assembly by the program allows for calculations to be performed within nodes, hence the summation of resulting nodal average values yield the final assembly average values. The obtained parameters are lastly normalized to 1 ton of initial heavy metal $[t; tHM]$[14].
In the aim of the thesis, the following models are utilized by SNF in order to apprehend the above mentioned physical properties/parameters.

- The use of isotope concentration models on the basis of library isotope data tables for the calculations of end-of-life-EOL[18] isotopic concentrations.
- The power history[19] model deduces the dependence of nodal power history on the nodal EOL isotope concentration.
- Decay models consisting of decay chain dependencies on CT yield final isotopic concentrations as a function of CT.
- Source terms models for the derivation of isotopic radiation source terms using final isotopic concentrations.

The data required for the model implementations is provided by SNF library (SNFlib*-) along with additional data and history file prepared with CASMO, CMSLINK and SIMULATE. The cross section library needed is obtained by CASMO which is a two dimensional fuel depletion (lattice physics)[20] code. The CMSLINK provides SIMULATE with the cross sectional data file from CASMO. SIMULATE, a thee dimensional diffusion equation solver for neutron flux on nodal segments of the assembly[14].

## A.2 SNF Input

An example of a typical SNF input used in the program to obtain the output results for the desired fuel assemblies.

[18]Time at which the fuel depletion is profound, the fuel is considered used up and is discharged.
[19]Information on fuel irradiation and reactor operation history is modeled and accounted for.
[20]Lattices are refereed to as the axial segmentation of fuel assemblies in order to simulate the flux distribution of photons and neutrons.

```
&NEWCASE
   TITLE   = 'TEST R1'
   LIBFILE ='E:/SNF/data/lib/SNFlib-1.60.dat'
   RES_FIL ='E:\SNF\data\pool\20210222\r1\snf-7jan2019/snf_restart_r1_FuelwoHist-tot.hms'
   HIS_TYPE = 'RES' 'POOL'
   COBALT  =10, NITRO=100, CHLOR=5        ! Structure+impurities
   TIMEC = 1,2,3,4,5,6,7,8,9,10,12,15,20,25,30,35
   UNTS= 'YRS'
   UNACT   ='CI'
   LEVEL   ='AVER'
   SUMMARY     = OFF
   TITLE   = 'R-05-62 0710'
   FAID    = '0710'
   DCDATE = 22 07 1982
   ! TODATE = 23 03 2004
   NORM='ABS'
&END

&NEWCASE
   TITLE   = 'R-05-62 0900'
   FAID    = '0900'
   DCDATE = 22 07 1982
   ! TODATE = 18 02 200
NORM='ABS'
&END

&NEWCASE
   TITLE   = 'R-05-62 1136'
   FAID    = '1136'
   DCDATE = 18 06 1983
   ! TODATE = 09 02 2004
NORM='ABS'
&END
```

Figure 14: Example of SNF input used in running the SNF program.

In figure 14 the first rows of the input are intended to retrieve the SNF library files associated with the particular SNF version used. The history files and cross section libraries needed for the initial condition of the system are collected within the RES_FIL command. The TIMEC denotes all the cooling times at which the output hence the properties described above are evaluated. The standard unit for CT is set to years since the change in nuclear properties are well captured within that time frame. The obtained values to be presented in the output are averaged by the use of LEVEL=AVER. FAID denotes the fuel assembly ID and is unique, DCDATE is the fuel assembles discharge date and TODATE is the date of evaluation. In addition the resulting values are normalized by the absolute unit. In every new sequence initiate with &NEWCASE an additional fuel assembly is added, evaluated and for which the results are attained in the output.

# B Los Alamos National Laboratory's Monte Carlo N particle Simulator Version 5

## B.1 Overview

The Monte Carlo N particle transport code simulates individual particles by tracking them from and to events until their termination through processes such as absorption occurs. The transportation of particles between events such as collisions is considered to be differential in both space and time. Steps of individual particles are governed by Monte Carlo principal of random walk. Following each step of the particle is an evaluation of the probability regarding events by conditions that need to be meet for the events to occur. Probability distributions

of events are sampled through the selection of random number to determine the outcome of the particle for every step. Aspects or tallies[21] of the individual particles behavior are recorder throughout the simulation and averaged to yield the final MCNP result[10].

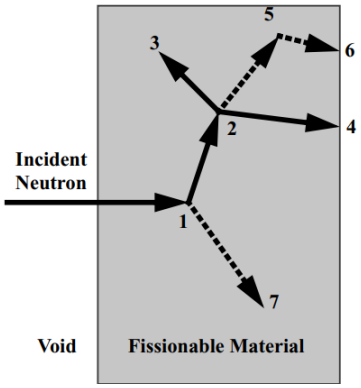


Figure 15: Illustration of the principal governing the MCNP process[10]

The principal governing the MCNP transport of a neutron in fissionable material is illustrated in figure 15, where also the particles random history is observed. Some number between 0 and 1 is selected randomly in order to determine if and where interaction occurs with respect to the physical properties of the particle in the simulation, probabilities of events and the material involved. The neutron collides at event 1 and is scattered with some direction determined by the physical scattering distribution. Along with the scattered neutron, a photon is also produced and is momentarily stored. The scattered neutron interacts at event 2 through fission which produces two outgoing neutrons and a photon. The one neutron and photon are stored while at event 3 the first fission neutron is captured and hence terminated. The stored neutron leaks out of the slab at event 4. Then the stored fission- photon is retrieved and collides at event 5, after which it leaks out at event 6. Lastly the first event photon is captured at event 7 completing the neutron history. Each Monte Carlo random walk is associated with a tally score $x_i$, where index i is the $i^{th}$ random walk. If the tally chosen by the user is energy deposition $x_i$ will be the energy deposition for the $i^{th}$ random walk. The probability function for some random walk of score x is unknown hence so is also the true mean or expected value $E[x]$ of that function. Instead the sampled mean $\bar{x}$

$$\bar{x} = \frac{1}{N}\sum_{i=1}^{N} x_i,$$

where $x_i$ is a value considered to be sampled from the unknown probability function, $N$ number of histories in the simulation, is taken to be an estimate of the true mean[10].

[21]There are several tallies which are related to particle current, particle flux and energy deposition by the user. The majority of the tallies are normalized with the number of starting particles.

Thereafter by the Strong Law of Large Numbers[22] the increase in $N$ number of histories converges the estimated mean $\bar{x}$ to the true $E[x]$. This allows for the particle simulation to represent the particle system. The deviation between true and estimated mean better known as the accuracy is referred to as systematic error and is hardly known. The user is therefore unaware if the simulation will accurately model the physical realty of the problem.
The variance of the sampled tally scores derived for large $N$ as following

$$S^2 = \frac{\sum_{i=1}^{N}(x_i - \bar{x})^2}{N-1} \approx \bar{x^2} - \bar{x}^2,$$

where $S$ is hence the estimated standard deviation while the variance of the estimated mean $\bar{x}$ is

$$S_{\bar{x}}^2 = \frac{S^2}{N}.$$

The precision $S_{\bar{x}}^2$ is considered to be a measure of the uncertainty in the estimated mean $\bar{x}$ afflicted by the variance and is caused by failure to sample portions of phase space that are important. From the expression above it is seen that the reduction of $S_{\bar{x}}^2$ is possible by increasing $N$ which can become computationally heavy or decreasing $S$. MCNP presents together with tally results the estimated relative error

$$R \equiv \frac{S_{\bar{x}}}{\bar{x}},$$

interpreted as the precision in relation to the estimated mean and are used as quality evaluation of the tallies[10].

## B.2 MCNP input

The MCNP input format is displayed in the sequential series of figures below. They show the input for PWR $15x15$ fuel assembly defining material composition, geometry; cell and surfaces and lastly tallies in.

[22] Assuming the true mean is finite the theorem states that if repeating the same experiment large number of times then the obtained average will converge to the true mean of the distribution.

```
C Modellering av ett knippe
C Celler, kuts, kapsling och vatten (uran och ledror)
1 3  -10.29    -11          u=1                $ Uran
3 0            11 -12       u=1                $ Mellan stav o kapsling
4 5  -6.6      12 -13       u=1                $ Kapsling
5 1  -1.0      13           u=1                $ luft runt kapslingen
6 1  -1.0      -14          u=2                $ Ledror, innsida
7 5  -6.6      14 -15       u=2                $ Ledror
8 1  -1.0      15           u=2                $ Vatten runt ledror
9 0            -16      lat=1 u=3 fill=-7:7 -7:7 0:0
      1 1 1 1 1 1 1 1 1 1 1 1 1 1 1
      1 1 1 1 1 1 1 1 1 1 1 1 1 1 1
      1 1 1 1 2 1 1 2 1 1 2 1 1 1 1
      1 1 1 1 1 1 1 1 1 1 1 1 1 1 1
      1 1 2 1 1 1 1 1 1 1 1 2 1 1 1
      1 1 1 1 2 1 1 1 2 1 1 1 1 1 1
      1 1 1 1 1 1 1 1 1 1 1 1 1 1 1
      1 1 2 1 1 1 1 2 1 1 1 1 2 1 1
      1 1 1 1 1 1 1 1 1 1 1 1 1 1 1
      1 1 1 1 1 2 1 1 1 2 1 1 1 1 1
      1 1 2 1 1 1 1 1 1 1 1 1 1 1 1
      1 1 1 1 1 1 1 1 1 1 1 1 2 1 1
      1 1 1 1 2 1 1 2 1 1 2 1 1 1 1
      1 1 1 1 1 1 1 1 1 1 1 1 1 1 1
      1 1 1 1 1 1 1 1 1 1 1 1 1 1 1
10 0             -17  u=4     fill=3
11 1  -1.0        17  u=4
c
c
12 0 -9 5 -8 fill=4
201 1 -1.0 -9 (-5:8)
18 2 -7.9 9 -10
19 0 10 -1
13 2 -7.9 1 -2
14 1 -1.0 2 -4 -5
15 1 -1.0 2 -4  8
16 0 4
17 1 -1.0 46 -4 5 -8
```

(a) MCNP input: First part.

```
c
20  1  -1  5  -6  2  -21
21  1  -1  5  -6  21  -22
22  1  -1  5  -6  22  -23
23  1  -1  5  -6  23  -24
24  1  -1  5  -6  24  -25
25  1  -1  5  -6  25  -26
26  1  -1  5  -6  26  -27
27  1  -1  5  -6  27  -28
28  1  -1  5  -6  28  -29
29  1  -1  5  -6  29  -30
30  1  -1  5  -6  30  -31
31  1  -1  5  -6  31  -32
32  1  -1  5  -6  32  -33
33  1  -1  5  -6  33  -34
34  1  -1  5  -6  34  -35
35  1  -1  5  -6  35  -36
36  1  -1  5  -6  36  -37
37  1  -1  5  -6  37  -38
38  1  -1  5  -6  38  -39
39  1  -1  5  -6  39  -40
40  1  -1  5  -6  40  -41
41  1  -1  5  -6  41  -42
42  1  -1  5  -6  42  -43
43  1  -1  5  -6  43  -44
44  1  -1  5  -6  44  -45
45  1  -1  5  -6  45  -46
50  1  -1  6  -7  2  -21
51  1  -1  6  -7  21  -22
52  1  -1  6  -7  22  -23
53  1  -1  6  -7  23  -24
54  1  -1  6  -7  24  -25
55  1  -1  6  -7  25  -26
56  1  -1  6  -7  26  -27
57  1  -1  6  -7  27  -28
58  1  -1  6  -7  28  -29
59  1  -1  6  -7  29  -30
60  1  -1  6  -7  30  -31
61  1  -1  6  -7  31  -32
```

(b) MCNP input: Second part.

```
11 CZ  0.4647   $ Kutspelare
12 CZ  0.4742    $ Kapsling, inner
13 CZ  0.5360    $ Kapsling, ytter
14 CZ  0.6335    $ Ledror, inner
15 CZ  0.677    $ Ledror,ytter
16 box   -0.715  -0.715 -1     1.43 0 0   0  1.43 0   0 0 368.43   $ 15.24 $ box runt stav
17 box   -10.7  -10.7 -1    21.4 0 0   0 21.4 0   0 0 368.43   $ 15.24 $ Knippet
c
1 cz 22.5
2 cz 22.8
3 cz 56
4 cz 150
5 pz -50
6 pz  120
7 pz  250
8 pz  420
9 cz 16.5
10 cz 16.8
c
21  cz  23
22  cz  24
23  cz  25
24  cz  26
25  cz  27
26  cz  28
27  cz  29
28  cz  30
29  cz  31
30  cz  33
31  cz  35
32  cz  37
33  cz  39
34  cz  41
35  cz  44
36  cz  47
37  cz  50
38  cz  53
39  cz  56
```

(c) MCNP input: Third part.

```
40  cz  59
41  cz  62
42  cz  65
43  cz  68
44  cz  71
45  cz  75
46  cz  80

m1 1001 2 8016 1
m2 24000 0.08 28000 0.18 26000 0.74
m3 92235 -0.0112 92238 -0.87 8016 -0.1188
m5    40000  -0.9885   41093  -0.01
       8016  -0.0012   26000  -0.0003     $ M5
c MESH
FMESH104:p geom=cyl origin 0 0 50 axs 0 0 1 vec 0 1 0
     IMESH= 37.8 87.8 IINTS=1 10                          $$15cm f kalorimetern
     JMESH= 350  JINTS=1
     KMESH= 1 KINTS=72                                    $$5 grader bitar
c
mode p
nps 1e7
imp:p 1 12r 1 1 1 1 0 1 1 77r
sdef x=d3 y=d4 z=d1 erg=d2 par=2
si1 0 370
sp1 0 1
si3 -11 11
sp3 0 1
si4 -11 11
sp4 0 1
c
si2  0.4 $ CEN energies
     0.7
     1.0
     1.5
     2.0
     2.5
     3.0
```

(d) MCNP input: Fourth part.

Figure 16: MCNP input for PWR $15x15$ fuel assembly.

In the first three figures 16a, 16b, 16c and beginning of 16d showing one of the MCNP input used, the problem geometry is constructed through cell cards. The geometry is intended to describe the real life storage at CLAB, meaning a fuel assembly inserted in a calorimeter surrounded by water. The input is read from left to right, sequentially from the first row down to the last. The first column[23] in figure 16a labels the cell card by some unique number, the second column defines the material the cell consists of, the third refers to the density of

[23]The column which is at the outermost left side in the figure.

the cell, from the forth and ascending columns; the numeric labels for defined surfaces which bound the cell. The column initiated with $u$ refer to an universe which the cell belongs to. In the first seven rows of 16a the cell cards define the fuel rods which consist of uranium or water and fill out the space of universe one and two respectively. The rods are then used in the repeated structure or lattice to construct the fuel assembly hence representing the real life composition of the PWR $15x15$ fuel. Thereafter the space between the fuel assembly and inner radius of the cylindrical structure confining the calorimeter, meaning the test chamber and the calorimeters cylindrical shell is added to the geometry. A shield of vacuum between the calorimeter wall and the outside pool water is also seen added however more realistically this shield should be of polyurethane foam and is considered in other inputs.
In figure 16b the cell cards rigorously define the space outside the calorimeter. In 16c are the surface cards where all of the surfaces used for the cells boundaries are defined. The first column of the surface card contain its label while the second states the shape of the surface. Two surfaces are used; cz which is a cylindrical surface with axis along the z-direction and pz represents a surface plan parallel to the z-axis. The third column of the surface card gives the radius or cutoff of cylinder and plan respectively.
The material card is seen in 16d consisting of materials $m1 - m5$ which are the materials used in the build up of the cells. Then the MESH card is added in order to examine and obtain tally results angel or vertically distributed around the fuel assembly. In this case the MESH card is used for angular distribution of the results. Number of starting photons are set to $1e7$ which is statistically motivated to be reasonable considering partly that the tallies are average values. The importance card *imp* states the importance of every cell in the system and how valuable the tacking of the particles is in that cell. The source of the particles is defines in the *sdef* card through uniform distributions in Cartesian space.

```
si2  0.4 $ CEN energies
     0.7
     1.0
     1.5
     2.0
     2.5
     3.0
     4.0
sp2  0.0   $ CEN relative g-flux
     7.61E+15
     3.38E+15
     3.99E+14
     3.68E+13
     4.74E+13
     9.23E+11
     1.13E+11
c
print
*f2:p 2
c
f6:p 50 24i 75
fq6 f e
fm6 1.78e15
c
c f16:p (12 201 18) (13 14 15 17 20 24i 45 50 24i 75 80 24i 105
c sd16 1 r
fq16 f e
c
f26:p 12 (20 24i 45 50 24i 75 80 24i 105)
sd26 1 r
fq26 f e
c
f36:p (12 201 18 13 14 15 17 20 24i 45 50 24i 75 80 24i 105)
sd36 1
fq36 f e
```

Figure 17: MCNP input: Fifth part.

In figure 17 of the MCNP input the source photon energy spectrum with corresponding photon counts both obtained from SNF-output, are inserted in the $si2$ and $sp2$ cards respectively. Lastly the desired tallies along with cells for which the tallies are recorded. The physical properties the tallies yield are the energy deposition.

## B.3 BWR and PWR fuel assembly MCNP

The following illustrations of BWR and PWR fuel assembly models obtained from MCNP viewing the inside of the calorimeter from above.

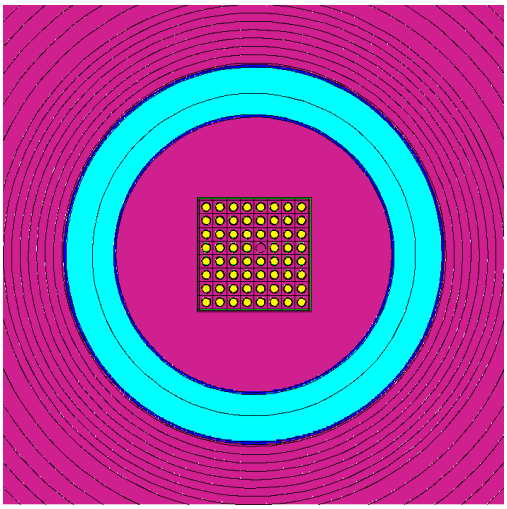

(a) BWR 8x8

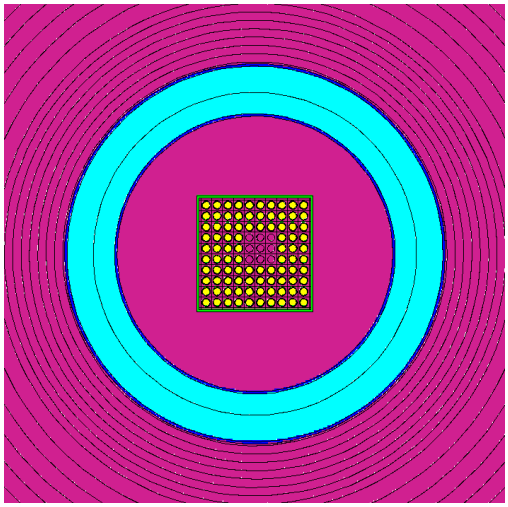

(b) BWR 10x10

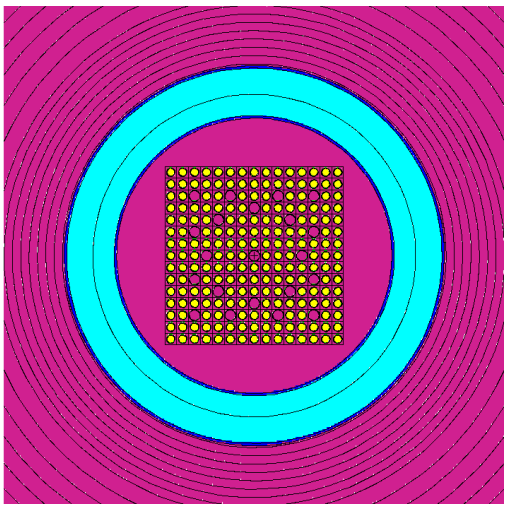

(c) PWR 15x15

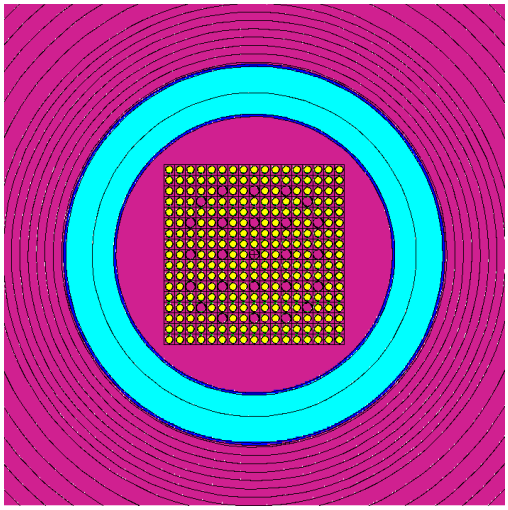

(d) PWR 17x17

Figure 18: BWR and PWR fuel assmebly models obtained from the MCNP program.

# C Uncertainty propagation

## C.1 Rules of propagating error

Rules for propagating error through a few basic arithmetic mathematical operations and natural logarithm. The uncertainty of a parameter is denoted with delta $\delta$ before the parameter notation.

$$z = x + y \Rightarrow \delta z = \sqrt{(\delta x)^2 + (\delta y)^2}, \tag{10}$$

$$z = c \cdot \frac{x}{y} \Rightarrow \frac{\delta z}{z} = \sqrt{(\frac{\delta x}{x})^2 + (\frac{\delta y}{y})^2}[13], \tag{11}$$

$$z = lnx \Rightarrow \delta(lnx) = \frac{\delta x}{x}[7]. \tag{12}$$

## C.2 Uncertainty of data in linear regression

The simple linear model with one independent variable $x$ estimating the data of y; $\hat{y}$, is considered.

$$\hat{y} = c + bx.$$

Standard error estimate $\sigma_{est}$ is defined as following

$$\sigma_{est} = \sqrt{\frac{\sum_{i=1}^{N}(y - \hat{y})^2}{N - 2}}, \tag{13}$$

where N is the number of data points. The uncertainty of the coefficient $b$ in the linear model is defined,

$$\delta b = \sqrt{\frac{\sigma_{est}^2}{\sum_{i=1}^{N} x_i^2 - N \cdot \bar{x}^2}}, \tag{14}$$

where $\bar{x}$ is the mean value of the data of the independent variable x[12].